Introducing planar hydrophobic groups into an alkyl-sulfonated rigid polyimide and how this affects morphology and proton conductivity

Yuki Nagao[a,*], Teppei Tanaka[a], Yutaro Ono[a], Kota Suetsugu[b], Mitsuo Hara[b], Guangtong Wang[a,c], Shusaku Nagano[d], Takashi Abe[e]

[a]School of Materials Science, Japan Advanced Institute of Science and Technology, 1-1 Asahidai, Nomi, Ishikawa 923-1292, Japan

[b]Department of Molecular and Macromolecular Chemistry, Graduate School of Engineering, Nagoya University, Furo-cho, Chikusa, Nagoya 464-8603, Japan

[c]Key Laboratory of Micro-systems and Micro-structures Manufacturing, Ministry of Education, Harbin Institute of Technology, Harbin 150001, China

[d]Nagoya University Venture Business Laboratory, Nagoya University, Furo-cho, Chikusa, Nagoya 464-8603, Japan

[e]Graduate School of Science and Technology, Niigata University, 8050 Ikarashi 2-no-cho, Niigata 950-2181, Japan

Corresponding author : ynagao@jaist.ac.jp (Y.N.)

Abstract

Effects on organized structure and proton conductivity by the introduction of hydrophobic groups into the sulfonated polyimide backbone were investigated. A new sulfonated random co-polyimide with ion exchange capacity (IEC) of 2.69 meq. g^{-1} was synthesized. In our previous reports, we demonstrated that alkyl-sulfonated polyimide (ASPI-2, IEC = 3.11 meq. g^{-1}) thin film consisting of pyromellitic dianhydride and 3,3′-bis(3-sulfopropoxy)benzidine exhibits the organized lamellar structure and high in-plane proton conduction over 10^{-1} S cm^{-1} based on a lyotropic liquid crystalline (LC) property. However, the origin of the lyotropic LC property in the sulfonated polyimide thin films was not clear. In this paper, 20% hydrophobic o-tolidine was introduced into the ASPI-2 polymer backbone to suppress the lyotropic LC property. To discuss the effect on the organized structure and proton conductivity by the introduction of the hydrophobic

groups, domain size, internal nanostructure, proton conductivity, water uptake, and proton dissociation from sulfonic acid groups were investigated by polarized optical microscopy, grazing incidence small-angle X-ray scattering, impedance measurements, quartz crystal microbalance, and Fourier transform infrared spectroscopy. The random co-polyimide thin film exhibited the birefringence and in-plane oriented lamellar structure. The lamellar distance was expanded up to 3.0 nm by water uptake. The lamellar expansion, molecular ordering, and proton dissociation showed similar behaviors by water uptake compared to the previous ASPI-2 thin film. Proton conductivity and water uptake per sulfonic acid group exhibited relatively high value of 3.2×10^{-2} S cm^{-1} and 12.5 at relative humidity (RH) = 95% and 298K. The estimated mobility of proton carriers decreased by 74% at λ = 12.5. Results suggest that the 20% substitution by hydrophobic monomers does not affect the structural difference but leads to the strong mobility decrease of proton carriers rather than the decrease of number of density.

Keywords: sulfonated polyimide; thin film; organized structure; proton conductivity; lyotropic liquid crystalline property

1. Introduction

Research on constructing ion conducting channels based on hierarchical structures by organizing molecules and macromolecules is attracting attention [1-7]. In nature, higher order structures such as proteins control the ion conductive channels and realize the response of ion conduction by external stimulus. Brinke, Ikkala and co-workers demonstrated switchable proton conduction by hierarchical order-disorder and order-order transitions [8]. Kato and co-workers also demonstrated switchable ionic conduction induced by a rectangular-hexagonal phase transition in wedge-shaped liquid-crystalline (LC) ammonium salts [9]. The utilization of self-assembled LC structure and self-organized LC orientation offers a useful approach for three dimensional controls of the ion conductive channels [4, 10-12]. Other groups have also reported relations between ionic conductivity and LC structure with thermotropic and lyotropic liquid crystal properties [13-16].

Several groups reported on an enhancement of proton conductivity in dimensional structure systems. In 1D structures, Kawakami and co-workers demonstrated the high proton conductivity by aligned electrospun nanofibers [17, 18]. Elabd and co-workers also reported on the high proton conductivity using Nafion nanofibers [19]. In 2D

structures, Brinke, Ikkala and co-workers reported on the lamellar-within-lamellar superstructure for anisotropic proton conduction [20]. Matsui and co-workers demonstrated highly anisotropic proton conduction in a well-defined lamellar structure in Langmuir-Blodgett films [21-23]. Other researchers showed 2D hierarchical system by layer-by-layer techniques for proton conduction [24-26]. In 3D structure, Kato and co-workers reviewed many types of self-organized structures based on the LC property [4, 11, 12].

Sulfonated polyimides are one of the promising candidates for essential polymer electrolytes because of their thermal and chemical stabilities [3, 27-46]. In our previous works, some sulfonated polyimide thin films showed organized lamellar structures with high proton conductivity over 10^{-2} S cm^{-1} at 298K [47-52]. To elucidate the origin of the high proton conductivity in the sulfonated polyimide thin films, four sulfonated polyimides with planar and bent backbones were investigated [51]. Results showed that both thin films with planar and bent backbones show an in-plane oriented lamellar structure. However, the proton conductivity of thin films with planar backbones exhibited higher values over 10^{-1} S cm^{-1} than that of thin films with bent backbones. The molecular ordering was enhanced in the case of planar backbones. These results suggest that the planar backbone is preferable for high proton conductivity. Krishnan and co-workers

found that the proton conductivity strongly depends on the molecular weight of the sulfonated polyimides with planar backbones [49]. They concluded that higher molecular weight enhances the molecular ordering of the in-plane oriented lamellar structure. Recently Takakura and co-workers investigated the sulfonated polyimide thin films with semi-aliphatic planar backbones [52]. The semi-aliphatic backbone induced less molecular ordering because of suppressed π-stack aggregation of the main chains in the lyotropic lamellar structure. However, the origin of the lyotropic LC property is not yet clear. In this paper, planar and hydrophobic o-tolidine was introduced into the polymer backbone to suppress the lyotropic LC property as shown in Fig. 1.

Figure 1. Comparison between our previous and present works.

The objective of the present study is to look into the effect of the planar hydrophobic groups on the organized structure and proton conductivity. Domain size, internal nanostructure, proton conductivity, water uptake, and proton dissociation from sulfonic acid groups were investigated by polarized optical microscopy (POM), RH-controlled *in-*

situ grazing incidence small-angle X-ray scattering (GISAXS), RH-controlled *in-situ* impedance measurements, RH-controlled *in-situ* quartz crystal microbalance (QCM), and RH-controlled *in-situ* Fourier transform infrared spectroscopy (FTIR). The structural analogy was observed compared to the previous sulfonated polyimide thin film. Only transport property changed by the 20% substitution of hydrophobic monomers into the main chain backbone. Results suggest that the introduction of hydrophobic monomers does not induce the structural change but leads to the strong mobility decrease of proton carriers rather than the decrease of number of density of proton carriers in this system.

2. Experimental section

2.1 Materials

3,3'-Dihydroxybenzidine, 1,3-propanesultone, pyromellitic dianhydride (PMDA), and *o*-tolidine (o-TOL) were used as received from Tokyo Chemical Industry Co. Ltd., Japan. Acetic acid, acetic anhydride, hydrochloric acid, sodium hydroxide, ethanol, acetone, and methanol were purchased from Wako Pure Chemical Ind. Ltd., Japan. *m*-Cresol and trimethylamine (TEA) (Kanto Chemicals Co. Ltd., Japan) were used as received. An

alkyl-sulfonated monomer, 3,3′-bis(3-sulfopropoxy)benzidine (3,3′-BSPB), was synthesized according to our literature [49].

2.2 Synthesis of a sulfonated random co-polyimide with hydrophobic groups

In this study, the effect of hydrophobic groups in the main chain was investigated for the relation between the organized structure and proton conductivity. Scheme 1 shows the synthetic route for the sulfonated random co-polyimide with hydrophobic monomers in the main chain. As a hydrophobic monomer, o-TOL was introduced into the main chain. The molar ratio of 3,3′-BSPB and o-TOL is 4:1 (20% substitution by o-TOL into the main chain backbone). The obtained sulfonated random co-polyimide is denoted as PMDA-3,3′-BSPB/o-TOL (4/1) according to the literature [53].

Scheme 1. Synthesis of PMDA-3,3′-BSPB/o-TOL (4/1).

For the synthesis of PMDA-3,3′-BSPB/o-TOL (4/1), 3,3′-BSPB (0.8 mmol), o-TOL (0.2 mmol), TEA (2.1 mmol), and 10 ml of *m*-cresol were placed in three-necked flask equipped with magnetic stirring and argon inset. The mixture was stirred at 80°C. After a

clear solution was obtained, PMDA (1 mmol) was added into the mixture. The mixture was heated at 180°C for 12 h. After cooling, the mixture was poured into cooled acetone. The precipitate was collected and washed several times with acetone, and dried at 100°C under reduced pressure for 12 h to obtain ammonium salt of PMDA-3,3′-BSPB/o-TOL (4/1). In our previous study, ion exchange process using Amberlyst was carried out. But a partially decomposed polyimide was obtained in the case of PMDA-3,3′-BSPB/o-TOL (4/1). Therefore the polymerized product was immersed in ethanol containing 1 mol/l HCl for 12 h. The acidification procedure was repeated three times followed by washing with pure ethanol. After drying at 80°C under vacuum pressure for 12 h, PMDA-3,3′-BSPB/o-TOL (4/1) in acid form was obtained. The chemical structure and composition ratio were confirmed by ^{1}H NMR spectrum. Peak assignments were shown in Fig. 2. Peaks at δ = 1.2 and 3.4 ppm correspond to the remaining TEA. Based on the integration of these peaks, degree of the protonation was found to be 97%. Peaks at δ = 2.5 and 4.6 ppm are corresponding to DMSO-d_6 and included water, respectively. No peak of the polyamic acid was found. Fig. 3 shows the Fourier transform infrared (FTIR) spectrum. Two strong absorptions for imide groups were observed at 1720 and 1380 cm^{-1}. These were assigned as asymmetric C=O stretching and C-N stretching vibration modes, respectively [48, 54, 55]. The characteristic absorption bands of the sulfonic acid groups

appeared between 1030 cm^{-1} and 1250 cm^{-1}. The observed vibrational mode at 1504 cm^{-1} is attributed to the phenyl C−C stretching vibration. No peak corresponds to the presence of the polyamic acid. Molecular weight of PMDA-3,3′-BSPB/o-TOL (4/1) determined by gel permeation chromatography showed 1.1×10^6.

Figure 2. ^{1}H NMR spectrum of PMDA-3,3′-BSPB/o-TOL (4/1).

Figure 3. IR spectrum of PMDA-3,3′-BSPB/o-TOL (4/1).

2.3 Preparation of thin films

Active ACT-200 spin-coater was used to prepare the thin films on Si and SiO_2 substrates. The substrates were cleaned prior to the film deposition. Plasma treatment was performed using a vacuum plasma system (Cute-MP; Femto Science Inc., Korea) to obtain surface hydrophilicity of the substrate. Thicknesses of the thin films were measured using atomic force microscope (AFM, VN-8000; Keyence Co.) and white-light interferometric microscope (BW-S506; Nikon Corp.). Thickness of the thin films was ca. 500 nm.

2.4 Observation of POM images

POM was conducted with crossed polarizers to observe the LC optical ordered domains in the polymer thin films (BX-51-P and DP28 camera; Olympus Corp.) Data were recorded with Cellscan controller software. All POM observations were conducted at room temperature and ambient humidity.

2.5 GISAXS measurements

Relative humidity (RH) controlled *in-situ* GISAXS measurements were performed using an X-ray diffractometer (ER-E; Rigaku Corp.) with an R-AXIS IV two-dimensional (2D) detector. The sample stage was composed of the goniometer and a vertical stage (ATS-C3316-EM/ALV-300-HM; Chuo Precision Industrial Co. Ltd.) with a humidity–controlled cell. The typical cell holds Lumilar windows to control humidified atmosphere around thin films. Nitrogen carrier gas was used as received without further dehumidification. Cu Kα radiation (λ = 0.1542 nm) with a beam size of approximately 300μm×300μm was used. The camera length was 300 mm. The incidence angle was chosen in the range from 0.20° to 0.22°. For 1D OP and IP profiles, the integrated regions were taken between -0.5° to +0.5° as 2θ from the center (0°) and the width of 1° as 2θ, respectively.

2.6 Water uptake measurement by QCM

Water uptake was measured using an in-house RH-controlled *in-situ* QCM system. QCM substrates (QA-A9M-SIO2-S(M)(SEP); SEIKO EG&G Co. Ltd.) were connected to oscillation circuit with DC power supply and frequency counter (53131A; Agilent Technologies, Inc.). QCM substrate was placed in an in-house constructed humidity chamber with high-resolution RH sensor. Various humidity environments were produced using dry N_2 and humidity controller (BEL Flow; MicrotracBEL Corp.). The frequencies before and after spin-coating on the QCM substrate were recorded under the dry N_2 stream for determination of the mass of dry film by the following Sauerbrey equation as,

$$\Delta m = \frac{S\times\sqrt{\rho\mu}}{2\times F^2}\times(-\Delta F), \quad (1)$$

where S represents the electrode surface area, ρ and μ denote the quartz density and quartz shear modulus, and F stands for the fundamental frequency of QCM substrate.

The water content (λ) per sulfonic acid group was calculated as follows,

$$\lambda = \left(\frac{m}{m_0} - 1\right)\times\frac{EW}{M_{H_2O}}, \quad (2)$$

where m signifies the film mass at each RH, m_0 stands for the film mass of at RH = 0%, M_{H_2O} denotes the molecular mass of water molecule, and EW expresses the equivalent

weight.

2.7 Proton conductivity measurements

Proton conductivity of the thin film was examined through impedance spectroscopy measurements using a frequency response analyzer (SI1260; Solartron Anlytical) equipped with a high-frequency dielectric interface (SI1260; Solartron Analytical). RH and temperature were controlled using a computer-controlled environmental test chamber (SH-221; Espec Corp.). For thin film conductivity measurement, two-probe method was used to obtain in-plane proton conductivity parallel to the thin film. Gold contacts were used as electrodes with a porous gold paste (SILBEST No. 8560; Tokuriki Chemical Research Co. Ltd.). Impedance data were collected for frequencies between 1 Hz and 10 MHz, with an applied alternating potential of 50 mV. Thin-film conductivity (σ) was calculated as,

$$\sigma = \frac{d}{Rlt} \quad , (3)$$

where *d* signifies the distance between the gold electrodes, *R* denotes the resistance value obtained from the impedance, *l* and *t* respectively stand for the contact electrode length and the thickness of the film.

2.8 IR measurements under hydrated condition

Hydration process and dissociation state of protons from sulfonic acid groups were examined by RH-controlled *in-situ* FTIR measurements. The thin film on Si wafer was set in an in-house cell with CaF_2 windows. Transmission IR spectra were taken using an FTIR spectrometer (Nicolet 6700; Thermo Fisher Scientific Inc.) equipped with deuterium triglycine sulfate (DTGS) detector. The relative humidity (RH) was controlled by a humidity generator (me-40DP-2PLW; Micro Equipment Inc.).

3. Result and Discussion

3.1 POM observation

In our previous study with alkyl-sulfonated polyimides without inducing hydrophobic groups in the main chain, the organized lamellar structure due to the lyotropic LC property exhibited high in-plane proton conductivity [51]. To elucidate the LC domain morphologies on the thin film, POM observation was carried out. Fig. 4 shows POM images for the PMDA-3,3′-BSPB/o-TOL (4/1) thin films. The birefringence on the thin films was identified under cross polarized light when the sample was rotated from 0° to 45° with respect to the direction of polarized light. LC domain was observed and its optical domain size was ca. 10 μm determined from the size of bright regions where LC

polymer main chains monoaxially oriented. This size is comparable order to that in the previously reported alkyl-sulfonated polyimide (ASPI-2) thin film [49]. Result shows the PMDA-3,3′-BSPB/o-TOL (4/1) thin film has the LC domain. So RH-controlled *in-situ* GISAXS measurements were conducted to reveal the internal nanostructure in the thin film.

Figure 4. POM images of PMDA-3,3′-BSPB/o-TOL (4/1) thin films at 0°and 45°, respectively.

3.2 RH-controlled *in-situ* GISAXS measurements

To reveal the internal nanostructure of the PMDA-3,3′-BSPB/o-TOL (4/1) thin film, RH-controlled *in-situ* GISAXS measurements were carried out. GISAXS is a powerful tool for revealing molecular packings and molecular orderings [56]. Fig. 5 shows 2D scattering profiles in RH = 0, 40, 70, and 95% conditions. 2D scattering patterns clearly demonstrated the origin of the new scattering indicated as white arrow in Fig. 5d with increasing the RH. The scattering intensity of the semicircles was anisotropic unlike the isotropic amorphous halo scattering. This emergent of the new scattering in the OP

direction can be seen in the previous report [48].

Figure 5. The 2D GISAXS profiles of the PMDA-3,3′-BSPB/o-TOL (4/1) thin film at (a) RH = 0%, (b) 40%, (c) 70%, and (d) 95%, respectively.

Figure 6 shows humidity-dependent 1D GISAXS profiles in the both OP and IP directions. One RH-dependent scattering peak was observed in the OP direction at 2θ = 6.05° (1.5 nm) in the RH = 0% condition. With increasing RH, the scattering peak reached at 2θ = 2.9° (3.0 nm). Positions of the IP peak at 2θ = 5.38° (1.6 nm), 11.01° (0.80 nm) were unchanged by the RH change. These two peaks are attributable to the periodic monomer unit length in the main chain [57]. The small angle scatterings at 2θ = 3 – 5° in the IP direction were derived from the overlapped scatterings from the OP direction during the extraction process from the 2D image. These scatterings are originally derived from the OP direction, not from the IP direction. Results indicate that the PMDA-3,3′-BSPB/o-TOL (4/1) thin film has an in-plane oriented lamellar structure and lamellar distance can be expanded up to 3.0 nm by the humidity dependable lyotropic LC property. Though 20% hydrophobic monomers were introduced into the polymer backbone, the

structural similarity was found for organized lamellar structure, behavior of lamellar expansion, and degree of molecular ordering compared to the previous ASPI-2 thin film.

Figure 6. Humidity-dependent 1D GISAXS profiles in the (a) OP and (b) IP directions.

3.4 Water uptake

For the number of water molecules per sulfonic acid group ($\lambda = H_2O$ / $-SO_3H$), RH-controlled *in-situ* QCM was carried out. Fig. 7 shows RH dependence of the λ value for the PMDA-3,3′-BSPB/o-TOL (4/1) thin film. The λ value of the thin film increased by 12.5 with RH = 95%. For the lamellar structure, the scaling of the correlation length should be linear with the water volume fraction [58]. Fig. 8 shows the relation between the lamellar distance and number of water molecules per sulfonic acid groups for the PMDA-3,3′-BSPB/o-TOL (4/1) thin film. Result reveals that the adsorbed water molecules can linearly expand the lamellar distance up to 3.0 nm. This is the first report that lyotropic LC-like behavior could be observed in the sulfonated random co-polyimide thin films with the hydrophobic backbone. The 20% substitution by hydrophobic o-TOL monomers into the main chain backbone reduces amount of water uptake (λ) by 10%

compared to the previous ASPI-2 thin film.

Figure 7. Humidity dependences of the number of adsorbed water molecules per sulfonic acid group for the PMDA-3,3′-BSPB/o-TOL (4/1) thin film.

Figure 8. Number of adsorbed water dependence of the lamellar distance for the PMDA-3,3′-BSPB/o-TOL (4/1) thin film.

3.5 Proton Conductivity

Figure 9 shows RH dependence of proton conductivity for the PMDA-3,3′-BSPB/o-TOL (4/1) thin film. The proton conductivity of the thin film increased with RH and reached 3.2×10^{-2} S cm^{-1} at RH = 95% and 298 K. This value is relatively high, but is lower value compared to that (2.0×10^{-1} S cm^{-1}) of the ASPI-2 thin film [51]. The ion exchange capacity of the PMDA-3,3′-BSPB/o-TOL (4/1) and ASPI-2 is 2.69 and 3.11, respectively. The 20% substitution by hydrophobic o-TOL monomers into the main chain backbone reduces proton conductivity by 84%. The proton conductivity is proportional

to the number of density and mobility of proton carriers as follows [59, 60],

$$\sigma = n\mu e \ , (4)$$

where n signifies the number of density of proton carriers, μ stands for the mobility of proton carriers, and e is the elementary charge.

Figure 9. RH-dependent proton conductivity plots of the PMDA-3,3′-BSPB/o-TOL (4/1) thin film.

To discuss proton conductivity at the same amount of water uptake (λ) between PMDA-3,3′-BSPB/o-TOL (4/1) and ASPI-2 thin films [51], number of water molecule dependence of proton conductivity is shown in Fig. 10. Both PMDA-3,3′-BSPB/o-TOL (4/1) and ASPI-2 thin films showed similar curves. But the proton conductivity of PMDA-3,3′-BSPB/o-TOL (4/1) thin film was lower in the whole water uptake range. Results indicate that the 20% substitution by hydrophobic o-TOL monomers into the main chain backbone reduces proton conductivity in the whole water uptake range. From the water uptake dependence of proton conductivity, proton conductivity of the ASPI-2 thin film can be estimated at the point of 12.5 water molecules, which λ value is identical with that of the PMDA-3,3′-BSPB/o-TOL (4/1) thin film at RH = 95%. The estimated conductivity

is 1.6×10^{-1} S cm^{-1}. Based on the equation (4), the number of density (n) reduces by 20% through the introduction of hydrophobic groups. So the decrease of mobility (μ) is found to be 74% at λ= 12.5. Therefore we suggest that the introduction of hydrophobic o-TOL monomers strongly decreases the mobility of proton carriers rather than the number of density of proton carriers in this system.

Figure 10. Number of water molecules dependence of proton conductivity. PMDA-3,3′-BSPB/o-TOL (4/1) thin film (●) and ASPI-2 thin film (■) [51].

3.6 RH-controlled *in-situ* FTIR measurements

To evaluate the difference of hydration state and dissociation of proton from sulfonic acid groups between PMDA-3,3′-BSPB/o-TOL (4/1) and ASPI-2 thin films, RH-controlled *in-situ* FTIR measurements were conducted. Fig. 11 shows humidity-dependent FTIR spectra for the PMDA-3,3′-BSPB/o-TOL (4/1) thin films. The broad band between 2700 and 3700 cm^{-1} corresponds to OH stretching vibrations of adsorbed water molecules. The absorbance of the OH stretching mode increased with RH. The amount of adsorbed water based on the integration of OH band area matched with the

isotherm curve from QCM measurements. The peak position of the maximum absorbance was 3415 cm^{-1} at RH = 95%. This wavenumber is similar with that of the ASPI-2 thin film. IR result suggests that the 20% substitution by hydrophobic o-TOL monomers into the main chain backbone does not change the state of the hydrogen bonding networks at the hydrated state. Other bands were clearly observed at 1725, 1640, 1200, and 1035 cm^{-1} corresponding to the $\nu_{as}(C=O)$ of imide groups, $\delta(H\text{-}O\text{-}H)$, $\nu_{as}(SO_3^-)$, and $\nu_s(SO_3^-)$, respectively. The amount of dissociated protons can be discussed from the absorbance of the $\nu_s(SO_3^-)$ mode. This absorbance abruptly increased from RH = 0% to 20%. Protons can be easily deprotonated from the sulfonic acid groups with ca. 1.5 water molecules per sulfonic acid. The saturated absorbance under the high RH region suggests that all protons are deprotonated. So number of density is constant in the high RH region. Similar behavior was observed in the ASPI-2 thin film (Supporting Information in ref. [51]). These deprotonated protons can be considered as proton carriers to enhance the proton conductivity with water uptake.

Figure 11. RH-controlled *in-situ* FT-IR spectra of the PMDA-3,3′-BSPB/o-TOL (4/1) thin film. (a) Wavenumber range between 1000 – 4000 cm^{-1}. (b) Wavenumber range between 950 – 1850 cm^{-1}.

In our earlier works, we demonstrated that the in-plane oriented lamellar organized structure can contribute the high in-plane proton conduction in sulfonated polyimide thin films. In the present work, the influence of 20% substitution by hydrophobic o-TOL monomers into the main chain backbone was discussed on the organized structure and proton conductivity. The PMDA-3,3′-BSPB/o-TOL (4/1) thin film exhibits the in-plane oriented lamellar structure. The lamellar distance was expanded up to 3.0 nm by water uptake. In spite of the 20% substitution of hydrophobic monomers, the structure and structural change were found to be similar to the previous sulfonated polyimide thin film. Proton conductivity keeps relatively high value of 3.2×10^{-2} S cm^{-1} but it's value is lower than that of the previous ASPI-2 thin film in the whole water uptake range. The 20% substitution by hydrophobic o-TOL monomers does not change the state of hydrogen bonding networks in the high RH region. Compared to the previous ASPI-2 thin film, the number of density and mobility of the proton carriers were estimated from the obtained proton conductivity. The number of density should decrease by 20% because of the 20% substitution of hydrophobic monomers from sulfonated 3,3′-BSPB monomers. The mobility decreased by 74% at λ = 12.5. Results suggest that the introduction of hydrophobic o-TOL monomers leads to the strong mobility decrease of proton carriers

rather than the decrease of number of density in this system. Discussion on the mobility of proton carriers in thin film forms is still challenging compared to that in bulk forms because of the limitation of the measurement methods. These results can give a new opportunity to discuss proton mobility in thin film forms by tuning the different degree of substitution based on the structural similarity in future. Temperature dependence of the proton conductivity gives an opportunity to discuss the proton conduction mechanism, however, lyotropic LC phase depends on temperature. Before discussing temperature dependence of the proton conductivity, it is necessary to reveal temperature dependences of the organized structure and water uptake. Temperature dependence of the proton conductivity also gives a useful information about activation enthalpy and pre-exponential factor to discuss the mechanism between a simple percolation effect (related with pre-exponential factor) or an effect on the local mobility (related with activation enthalpy). This should be measured with a fixed λ value using a gas tight conductivity cell etc. This study is under investigation. Biaxially oriented thin films using these sulfonated polyimides with planar backbones may also contribute the further discussion on the proton mobility.

4. Conclusions

In this paper, the effect on the organized structure and proton conductivity by the substitution of planar hydrophobic groups in the main chain backbone was investigated. A new sulfonated polyimide, PMDA-3,3′-BSPB/o-TOL (4/1), was synthesized with 20% substitution by hydrophobic o-TOL monomers from the previous ASPI-2 backbone. The PMDA-3,3′-BSPB/o-TOL (4/1) thin film exhibited the organized lamellar structure from GISAXS results. The lamellar distance was expanded up to 3.0 nm by water uptake. This behavior can be explained by the lyotropic LC property. The structural analogy was found between the previous ASPI-2 and present PMDA-3,3′-BSPB/o-TOL (4/1) thin film. Only transport property changed by the 20% substitution of hydrophobic monomers into the main chain backbone. Results suggest that the introduction of hydrophobic o-TOL monomers does not induce the structural change but leads to the strong mobility decrease of proton carriers rather than the decrease of number of density.

Funding

The authors declare no competing financial interest.

Acknowledgement

Y.N. thanks Mr. Tetsuya Honbo, Mr. Ryo Takatani, and Mr Yao Yuze for their kind supports during preparation of manuscript. This work was supported in part by the Nanotechnology Platform Program (Molecule and Material Synthesis) of the Ministry of Education, Culture, Sports, Science and Technology (MEXT), Japan. This work was partially supported by JSPS KAKENHI Grant Number JP18K05257.

References

[1] K.D. Kreuer, On the development of proton conducting polymer membranes for hydrogen and methanol fuel cells, J. Membr. Sci. 185 (2001) 29.
[2] O. Ikkala, B.G. ten, Functional materials based on self-assembly of polymeric supramolecules, Science 295 (2002) 2407.
[3] M.A. Hickner, H. Ghassemi, Y.S. Kim, B.R. Einsla, J.E. McGrath, Alternative polymer systems for proton exchange membranes (PEMs), Chem. Rev. 104 (2004) 4587.
[4] T. Kato, N. Mizoshita, K. Kishimoto, Functional liquid-crystalline assemblies: Self-organized soft materials, Angew. Chem. Int. Ed. 45 (2006) 38.
[5] M.J. Park, N.P. Balsara, Anisotropic Proton Conduction in Aligned Block Copolymer Electrolyte Membranes at Equilibrium with Humid Air, Macromolecules 43 (2010) 292.
[6] G.A. Giffin, G.M. Haugen, S.J. Hamrock, V. Di Noto, Interplay between Structure and Relaxations in Perfluorosulfonic Acid Proton Conducting Membranes, J. Am. Chem. Soc. 135 (2013) 822.
[7] Y. Nagao, Proton-Conductivity Enhancement in Polymer Thin Films, Langmuir 33 (2017) 12547.
[8] J. Ruokolainen, R. Makinen, M. Torkkeli, T. Makela, R. Serimaa, G. ten Brinke, O. Ikkala, Switching supramolecular polymeric materials with multiple length scales, Science 280 (1998) 557.
[9] B. Soberats, M. Yoshio, T. Ichikawa, X. Zeng, H. Ohno, G. Ungar, T. Kato, Ionic Switch Induced by a Rectangular–Hexagonal Phase Transition in Benzenammonium

Columnar Liquid Crystals, J. Am. Chem. Soc. 137 (2015) 13212.
[10] T. Kato, M. Yoshio, T. Ichikawa, B. Soberats, H. Ohno, M. Funahashi, Transport of ions and electrons in nanostructured liquid crystals, Nat. Rev. Mater. 2 (2017) 17001.
[11] T. Kato, J. Uchida, T. Ichikawa, B. Soberats, Functional liquid-crystalline polymers and supramolecular liquid crystals, Polym. J. 50 (2017) 149.
[12] T. Kato, J. Uchida, T. Ichikawa, T. Sakamoto, Functional Liquid Crystals towards the Next Generation of Materials, Angew. Chem. Int. Ed. 57 (2018) 4355.
[13] Y. Chen, M.D. Lingwood, M. Goswami, B.E. Kidd, J.J. Hernandez, M. Rosenthal, D.A. Ivanov, J. Perlich, H. Zhang, X. Zhu, M. Möller, L.A. Madsen, Humidity-Modulated Phase Control and Nanoscopic Transport in Supramolecular Assemblies, J. Phys. Chem. B 118 (2014) 3207.
[14] J.J. Hernandez, H. Zhang, Y. Chen, M. Rosenthal, M.D. Lingwood, M. Goswami, X. Zhu, M. Moeller, L.A. Madsen, D.A. Ivanov, Bottom-Up Fabrication of Nanostructured Bicontinuous and Hexagonal Ion-Conducting Polymer Membranes, Macromolecules 50 (2017) 5392.
[15] I. Tonozuka, M. Yoshida, K. Kaneko, Y. Takeoka, M. Rikukawa, Considerations of polymerization method and molecular weight for proton-conducting poly(p-phenylene) derivatives, Polymer 52 (2011) 6020.
[16] J.H. Lee, K.S. Han, J.S. Lee, A.S. Lee, S.K. Park, S.Y. Hong, J.-C. Lee, K.T. Mueller, S.M. Hong, C.M. Koo, Facilitated Ion Transport in Smectic Ordered Ionic Liquid Crystals, Adv. Mater. 28 (2016) 9301.
[17] R. Takemori, G. Ito, M. Tanaka, H. Kawakami, Ultra-high proton conduction in electrospun sulfonated polyimide nanofibers, RSC Adv. 4 (2014) 20005.
[18] T. Tamura, H. Kawakami, Aligned Electrospun Nanofiber Composite Membranes for Fuel Cell Electrolytes, Nano Lett. 10 (2010) 1324.
[19] B. Dong, L. Gwee, l.C.D. Salas-de, K.I. Winey, Y.A. Elabd, Super Proton Conductive High-Purity Nafion Nanofibers, Nano Lett. 10 (2010) 3785.
[20] R. Maki-Ontto, M.K. de, E. Polushkin, E.G.A. van, B.G. ten, O. Ikkala, Tridirectional protonic conductivity in soft materials, Adv. Mater. 14 (2002) 357.
[21] T. Sato, M. Tsukamoto, S. Yamamoto, M. Mitsuishi, T. Miyashita, S. Nagano, J. Matsui, Acid-Group-Content-Dependent Proton Conductivity Mechanisms at the Interlayer of Poly(N-dodecylacrylamide-co-acrylic acid) Copolymer Multilayer Nanosheet Films, Langmuir 33 (2017) 12897.
[22] J. Matsui, H. Miyata, Y. Hanaoka, T. Miyashita, Layered Ultrathin Proton Conductive Film Based on Polymer Nanosheet Assembly, ACS Appl. Mater. Inter. 3 (2011) 1394.

[23] T. Sato, Y. Hayasaka, M. Mitsuishi, T. Miyashita, S. Nagano, J. Matsui, High Proton Conductivity in the Molecular Interlayer of a Polymer Nanosheet Multilayer Film, Langmuir 31 (2015) 5174.
[24] T.R. Farhat, P.T. Hammond, Designing a new generation of proton-exchange membranes using layer-by-layer deposition of polyelectrolytes, Adv. Funct. Mater. 15 (2005) 945.
[25] T. Tago, H. Shibata, H. Nishide, Membrane preparation of polysulfonic acid complexes by layer-by-layer adsorption, Macromol. Symp. 235 (2006) 19.
[26] Y. Daiko, K. Katagiri, K. Shimoike, M. Sakai, A. Matsuda, Structures and electrical properties of core-shell composite electrolytes with multi-heterointerfaces, Solid State Ionics 178 (2007) 621.
[27] S. Faure, N. Cornet, G. Gebel, R. Mercier, M. Pineri, B. Sillion, Sulfonated polyimides as novel proton exchange membranes for H2/O2 fuel cells, New Mater. Fuel Cell Mod. Battery Syst. II: Proc. of the 2nd Int. Symp., Ecole Polytechnique de Montreal, (1997), 818.
[28] N. Cornet, O. Diat, G. Gebel, F. Jousse, D. Marsacq, R. Mercier, M. Pineri, Sulfonated polyimide membranes: a new type of ion-conducting membrane for electrochemical applications, J. New Mat. Elect. Syst. 3 (2000) 33.
[29] C. Genies, R. Mercier, B. Sillion, N. Cornet, G. Gebel, M. Pineri, Soluble sulfonated naphthalenic polyimides as materials for proton exchange membranes, Polymer 42 (2001) 359.
[30] J.H. Fang, X.X. Guo, S. Harada, T. Watari, K. Tanaka, H. Kita, K. Okamoto, Novel sulfonated polyimides as polyelectrolytes for fuel cell application. 1. Synthesis, proton conductivity, and water stability of polyimides from 4,4 '-diaminodiphenyl ether-2,2 '-disulfonic acid, Macromolecules 35 (2002) 9022.
[31] X.X. Guo, J.H. Fang, T. Watari, K. Tanaka, H. Kita, K.I. Okamoto, Novel sulfonated polyimides as polyelectrolytes for fuel cell application. 2. Synthesis and proton conductivity, of polyimides from 9,9-bis(4-aminophenyl)fluorene-2,7-disulfonic acid, Macromolecules 35 (2002) 6707.
[32] S. Besse, P. Capron, O. Diat, G. Gebel, F. Jousse, D. Marsacq, M. Pineri, C. Marestin, R. Mercier, Sulfonated polyimides for fuel cell electrode membrane assemblies (EMA), J. New Mat. Elect. Syst. 5 (2002) 109.
[33] Y. Yin, J.H. Fang, Y.F. Cui, K. Tanaka, H. Kita, K. Okamoto, Synthesis, proton conductivity and methanol permeability of a novel sulfonated polyimide from 3-(2 ',4 '-diaminophenoxy)propane sulfonic acid, Polymer 44 (2003) 4509.
[34] Y. Yin, J.H. Fang, H. Kita, K. Okamoto, Novel sulfoalkoxylated polyimide

membrane for polymer electrolyte fuel cells, Chem. Lett. 32 (2003) 328.
[35] K. Okamoto, Sulfonated polyimides for polymer electrolyte membrane fuel cell, J. Photopolym. Sci. Tec. 16 (2003) 247.
[36] K. Miyatake, N. Asano, M. Watanabe, Synthesis and properties of novel sulfonated polyimides containing 1,5-naphthylene moieties, J. Polym. Sci. Pol. Chem. 41 (2003) 3901.
[37] Y. Yin, J.H. Fang, T. Watari, K. Tanaka, H. Kita, K. Okamoto, Synthesis and properties of highly sulfonated proton conducting polyimides from bis(3-sulfopropoxy)benzidine diamines, J. Mater. Chem. 14 (2004) 1062.
[38] T. Watari, J.H. Fang, K. Tanaka, H. Kita, K. Okamoto, T. Hirano, Synthesis, water stability and proton conductivity of novel sulfonated polyimides from 4,4'-bis(4-aminophenoxy)biphenyl-3,3'-disulfonic acid, J. Membr. Sci. 230 (2004) 111.
[39] Y. Yin, Y. Suto, T. Sakabe, S.W. Chen, S. Hayashi, T. Mishima, O. Yamada, K. Tanaka, H. Kita, K. Okamoto, Water stability of sulfonated polyimide membranes, Macromolecules 39 (2006) 1189.
[40] X.H. Ye, H. Bai, W.S.W. Ho, Synthesis and characterization of new sulfonated polyimides as proton-exchange membranes for fuel cells, J. Membr. Sci. 279 (2006) 570.
[41] N. Asano, M. Aoki, S. Suzuki, K. Miyatake, H. Uchida, M. Watanabe, Aliphatic/aromatic polyimide lonomers as a proton conductive membrane for fuel cell applications, J. Am. Chem. Soc. 128 (2006) 1762.
[42] K. Miyatake, T. Yasuda, M. Hirai, M. Nanasawa, M. Watanabe, Synthesis and properties of a polyimide containing pendant sulfophenoxypropoxy groups, J. Polym. Sci., Part A: Polym. Chem. 45 (2007) 157.
[43] O. Savard, T.J. Peckham, Y. Yang, S. Holdcroft, Structure-property relationships for a series of polyimide copolymers with sulfonated pendant groups, Polymer 49 (2008) 4949.
[44] A. Ito, T. Yasuda, T. Yoshioka, A. Yoshida, X. Li, K. Hashimoto, K. Nagai, M. Shibayama, M. Watanabe, Sulfonated Polyimide/Ionic Liquid Composite Membranes for CO2 Separation: Transport Properties in Relation to Their Nanostructures, Macromolecules 51 (2018) 7112.
[45] T. Yasuda, S.-i. Nakamura, Y. Honda, K. Kinugawa, S.-Y. Lee, M. Watanabe, Effects of Polymer Structure on Properties of Sulfonated Polyimide/Protic Ionic Liquid Composite Membranes for Nonhumidified Fuel Cell Applications, ACS Appl. Mater. Inter. 4 (2012) 1783.
[46] S.-Y. Lee, T. Yasuda, M. Watanabe, Fabrication of protic ionic liquid/sulfonated polyimide composite membranes for non-humidified fuel cells, J. Power Sources 195

(2010) 5909.
[47] K. Krishnan, T. Yamada, H. Iwatsuki, M. Hara, S. Nagano, K. Otsubo, O. Sakata, A. Fujiwara, H. Kitagawa, Y. Nagao, Influence of Confined Polymer Structure on Proton Transport Property in Sulfonated Polyimide Thin Films, Electrochemistry 82 (2014) 865.
[48] K. Krishnan, H. Iwatsuki, M. Hara, S. Nagano, Y. Nagao, Proton conductivity enhancement in oriented, sulfonated polyimide thin films, J. Mater. Chem. A 2 (2014) 6895.
[49] K. Krishnan, H. Iwatsuki, M. Hara, S. Nagano, Y. Nagao, Influence of Molecular Weight on Molecular Ordering and Proton Transport in Organized Sulfonated Polyimide Thin Films, J. Phys. Chem. C 119 (2015) 21767.
[50] Y. Nagao, K. Krishnan, R. Goto, M. Hara, S. Nagano, Effect of Casting Solvent on Interfacial Molecular Structure and Proton Transport Characteristics of Sulfonated Polyimide Thin Films, Anal. Sci. 33 (2017) 35.
[51] Y. Ono, R. Goto, M. Hara, S. Nagano, T. Abe, Y. Nagao, High Proton Conduction of Organized Sulfonated Polyimide Thin Films with Planar and Bent Backbones, Macromolecules 51 (2018) 3351.
[52] K. Takakura, Y. Ono, K. Suetsugu, M. Hara, S. Nagano, T. Abe, Y. Nagao, Lyotropic ordering for high proton conductivity in sulfonated semialiphatic polyimide thin films, Polym. J. 51 (2018) 31.
[53] Y. Yin, O. Yamada, Y. Suto, T. Mishima, K. Tanaka, H. Kita, K.-i. Okamoto, Synthesis and characterization of proton-conducting copolyimides bearing pendant sulfonic acid groups, J. Polym. Sci., Part A: Polym. Chem. 43 (2005) 1545.
[54] T. Miyamae, K. Tsukagoshi, O. Matsuoka, S. Yamamoto, H. Nozoye, Surface Characterization of Polyamic Acid and Polyimide Films Prepared by Vapor Deposition Polymerization by Using Sum-Frequency Generation, Langmuir 17 (2001) 8125.
[55] J. Sung, D. Kim, C.N. Whang, M. Oh-e, H. Yokoyama, Sum-Frequency Vibrational Spectroscopic Study of Polyimide Surfaces Made by Spin Coating and Ionized Cluster Beam Deposition, J. Phys. Chem. B 108 (2004) 10991.
[56] S. Nagano, Inducing Planar Orientation in Side‐Chain Liquid‐Crystalline Polymer Systems via Interfacial Control, Chem. Rec. 16 (2016) 378.
[57] J. Wakita, S. Jin, T.J. Shin, M. Ree, S. Ando, Analysis of Molecular Aggregation Structures of Fully Aromatic and Semialiphatic Polyimide Films with Synchrotron Grazing Incidence Wide-Angle X-ray Scattering, Macromolecules 43 (2010) 1930.
[58] K.-D. Kreuer, G. Portale, A Critical Revision of the Nano-Morphology of Proton Conducting Ionomers and Polyelectrolytes for Fuel Cell Applications, Adv. Funct. Mater.

23 (2013) 5390.
[59] A.K. Arof, S. Amirudin, S.Z. Yusof, I.M. Noor, A method based on impedance spectroscopy to determine transport properties of polymer electrolytes, Phys. Chem. Chem. Phys. 16 (2014) 1856.
[60] N.M.J. Rasali, Y. Nagao, A.S. Samsudin, Enhancement on amorphous phase in solid biopolymer electrolyte based alginate doped NH4NO3, Ionics Published online. (DOI:10.1007/s11581-018-2667-3) (2018).

List of Scheme and Figure captions

Figure 11. RH-controlled *in-situ* FT-IR spectra of the PMDA-3,3′-BSPB/o-TOL (4/1) thin film. (a) wavenumber range between 1000 – 4000 cm^{-1}. (b) wavenumber range between 950 – 1850 cm^{-1}.

Collection of Scheme and Figures

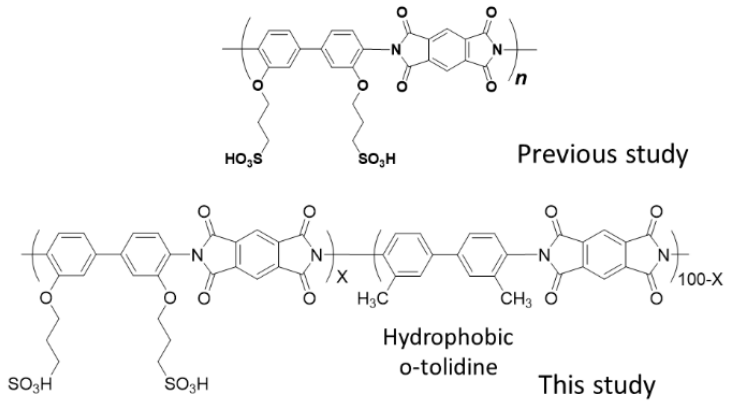

Figure 1. Comparison between our previous and present works.

Scheme 1. Synthesis of PMDA-3,3′-BSPB/o-TOL (4/1).

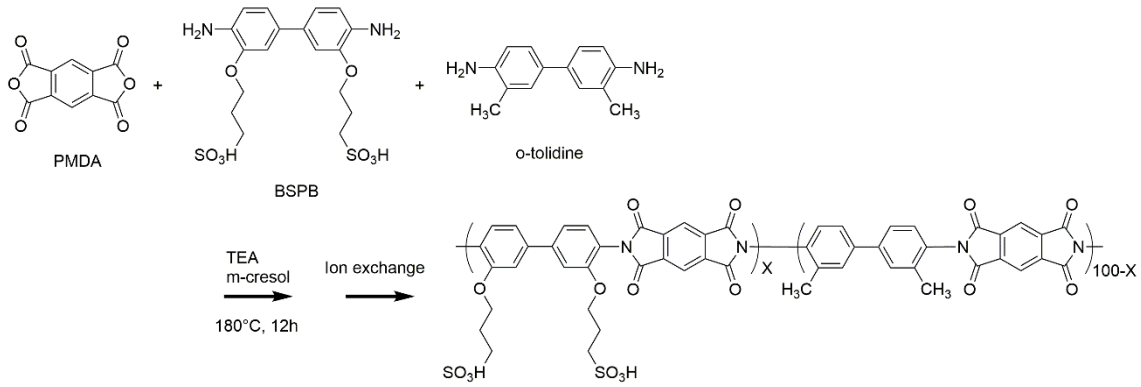

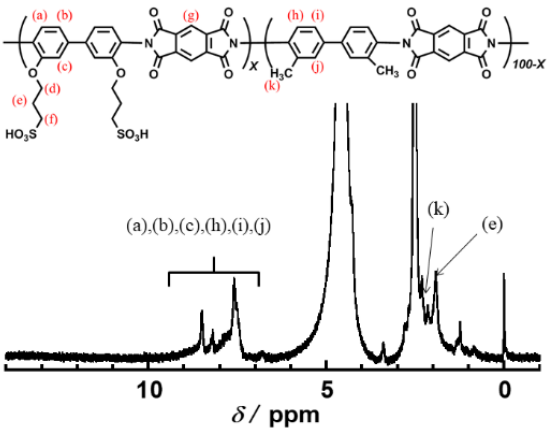

Figure 2. ^{1}H NMR spectrum of PMDA-3,3′-BSPB/o-TOL (4/1).

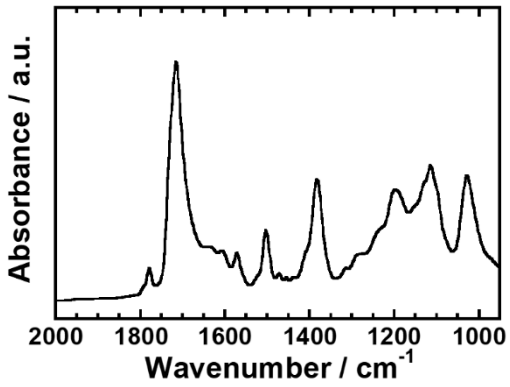

Figure 3. IR spectrum of PMDA-3,3′-BSPB/o-TOL (4/1).

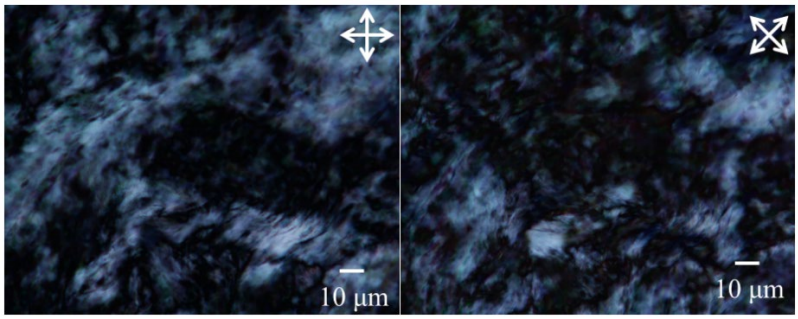

Figure 4. POM images of PMDA-3,3′-BSPB/o-TOL (4/1) thin films at 0°and 45°, respectively.

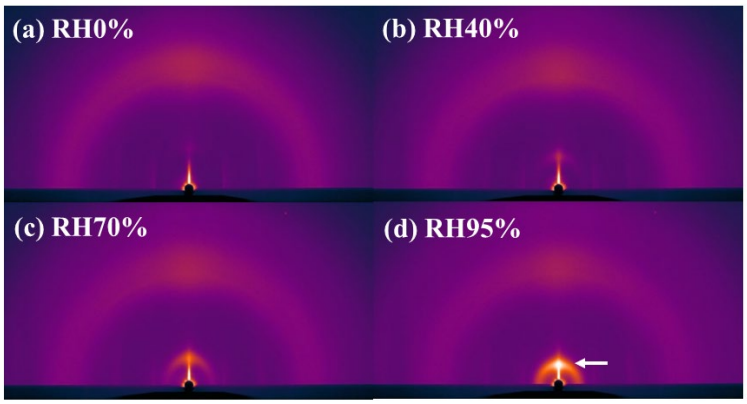

Figure 5. The 2D GISAXS profiles of the PMDA-3,3′-BSPB/o-TOL (4/1) thin film at (a) RH = 0%, (b) 40%, (c) 70%, and (d) 95%, respectively.

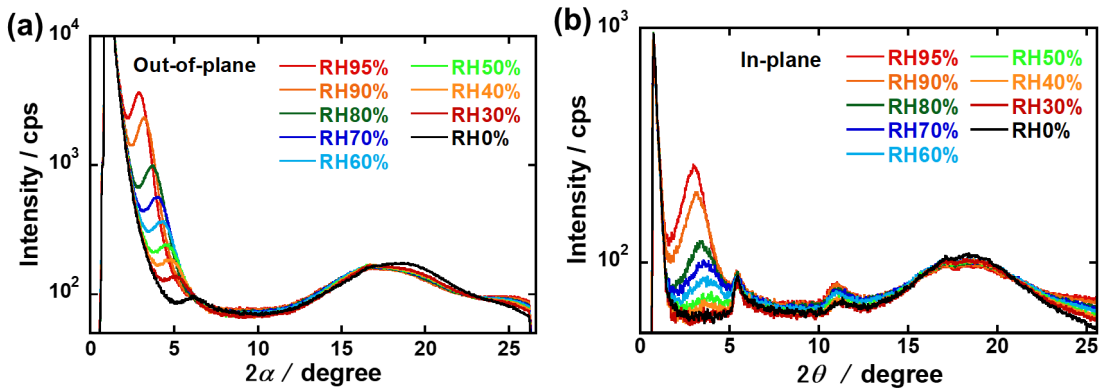

Figure 6. Humidity-dependent 1D GISAXS profiles in the (a) OP and (b) IP directions.

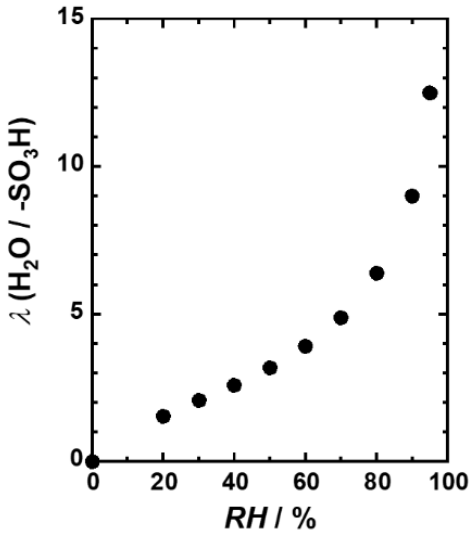

Figure 7. Humidity dependences of the number of adsorbed water molecules per sulfonic acid group for the PMDA-3,3′-BSPB/o-TOL (4/1) thin film.

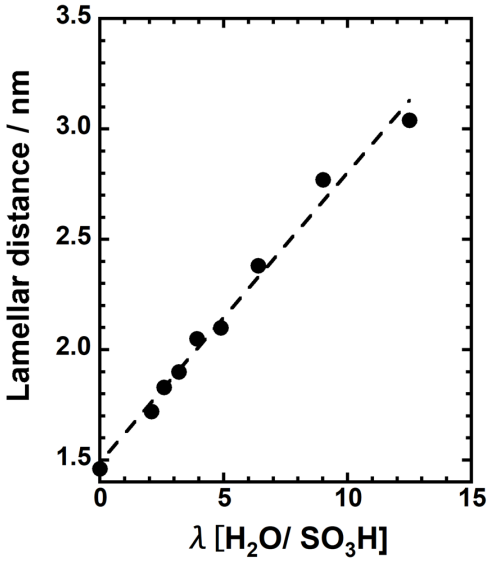

Figure 8. Number of adsorbed water dependence of the lamellar distance for the PMDA-3,3′-BSPB/o-TOL (4/1) thin film.

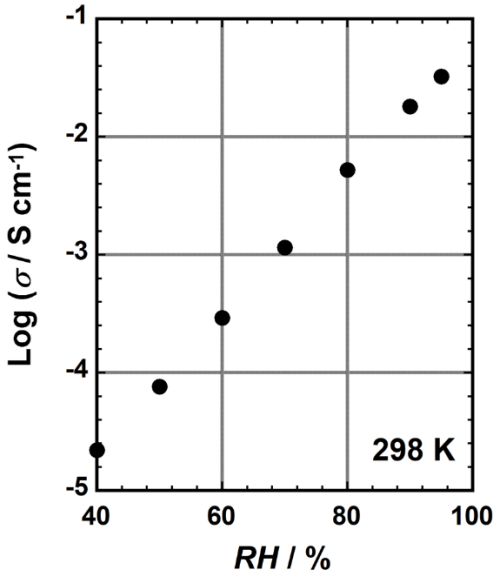

Figure 9. RH-dependent proton conductivity plots of the PMDA-3,3′-BSPB/o-TOL (4/1) thin film.

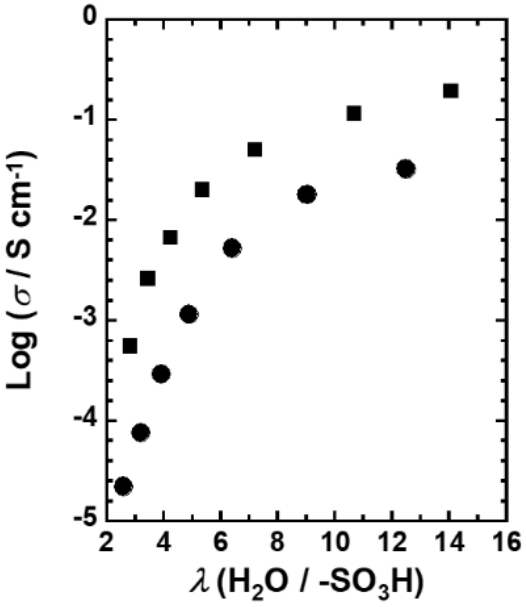

Figure 10. Number of water molecules dependence of proton conductivity. PMDA-3,3′-BSPB/o-TOL (4/1) thin film (●) and ASPI-2 thin film (■) [51].

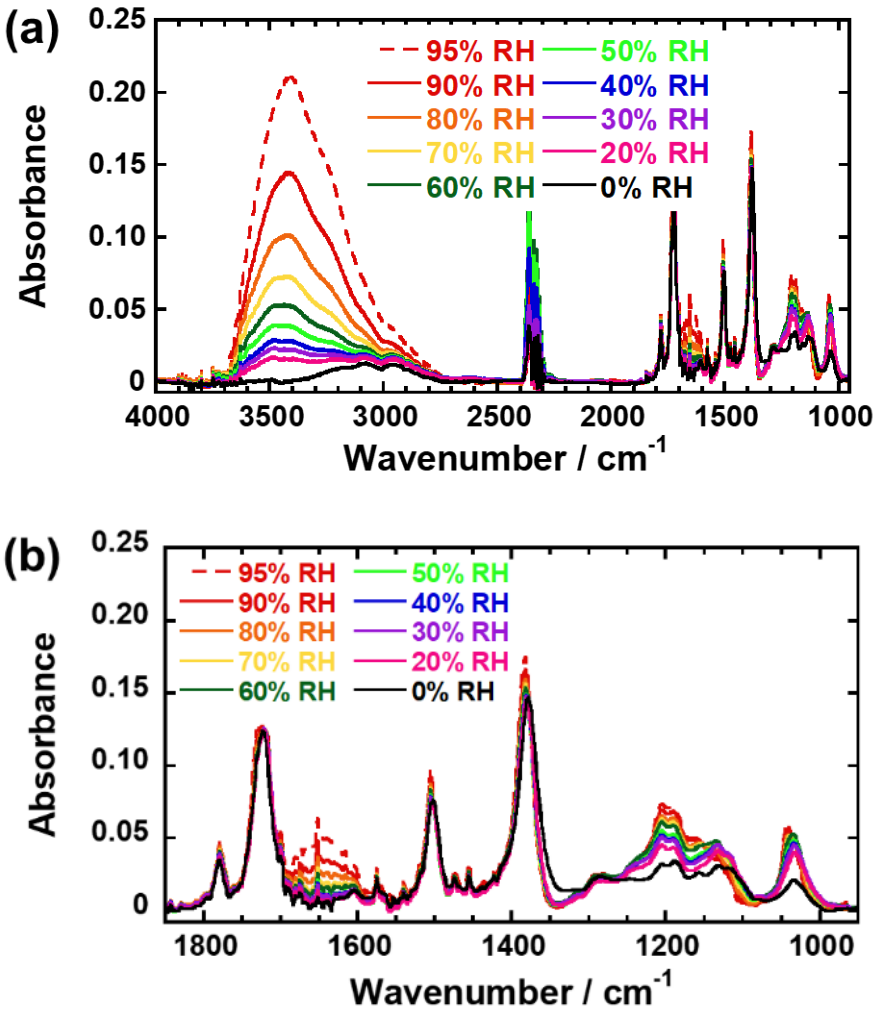

Figure 11. RH-controlled *in-situ* FT-IR spectra of the PMDA-3,3′-BSPB/o-TOL (4/1) thin film. (a) Wavenumber range between 1000 – 4000 cm^{-1}. (b) Wavenumber range between 950 – 1850 cm^{-1}.